

Supporting Information

Reversible Redox ^{19}F Magnetic Resonance Imaging Nanoprobes for Monitoring Redox State *in Vivo*

Xiaoyao Xiong, Sijia Li, Yumin Li, Suying Xu, Chang Guo and Leyu Wang**

State Key Laboratory of Chemical Resource Engineering, College of Chemistry, Beijing University of Chemical Technology, Beijing 100029, China.

E-mail: guoc@mail.buct.edu.cn; lywang@mail.buct.edu.cn

Table of Contents

1. Experimental Procedures.....	S3
2. Supplemental Figures and Tables.....	S8
3. Reference.....	S29

1. Experimental Procedures

Reagents and Chemicals. All solvents and chemicals were used as received without further purification. NaOH, NaCl, Na₂SO₄, KCl, dichloromethane, *N,N*-dimethylformamide, hexane, tetrahydrofuran, and absolute ethyl alcohol (EtOH) were supplied by Beijing Chemical Factory (Beijing, China). NaBH₄ was purchased from Tianjin Huadong Reagent Factory (Tianjin, China). 2,2'-diselanediyldiethanamine dihydrochloride and 2-iodo-1,1,1-trifluoroethane were purchased from Bidepharm (Shanghai, China). Hydrogen peroxide (H₂O₂, 30%, w/w) and poly(isobutylene-alt-maleic anhydride) were obtained from Sigma-Aldrich and Na₂S·9H₂O was obtained from J&K Scientific (Beijing, China). Nafion solution was supplied by Shanghai Hesen Electric Co., LTD (Shanghai, China). *N*-acetyl cysteine (NAC) was purchased from Beyotime Biotech. Inc.(Shanghai, China). All deuterium reagents used in the experiments were supplied by Beijing Innochem Science & Technology Co., LTD. (Beijing, China). Deionized (DI) water, obtained from a Millipore Milli-Q purification system, was used throughout all experiments.

Characterization. ¹H, ¹³C, ¹⁹F-NMR spectra were recorded on a Bruker Avance-III 400 MHz NMR spectrometer. ¹⁹F *T*₁ and *T*₂ relaxation time were measured on Bruker Avance-III 400 MHz NMR spectrometer with a coaxially D₂O-filled capillary tube for locking the field. The standard inversion-recovery (tir) pulse sequence and Carr-Purcell-Meiboom-Gill (CPMG) pulse sequence were used to measure ¹⁹F spin-lattice relaxation time (*T*₁) and spin-spin relaxation time (*T*₂), respectively. All MRI images were obtained on a 7.0 T Bruker Bio-Spec 70/30 MRI system. Dynamic light scattering (DLS) analysis was measured on a Zetasizer Nano-ZS90 zeta potential and size analyzer (Malvern). Transmission electron microscopy (TEM) images were acquired using a JEOL JEM-1200EX (100 kV). Mass spectra were measured on Xevo G2 Qtof mass spectrometer (Waters). Cyclic voltammetry curves were recorded on CHI 760E electrochemical workstation (CH Instruments). X-ray photoelectron spectroscopy was measured on ESCALAB 250Xi X-ray photoelectron spectrometer (Thermo Scientific).

Synthesis of 2-((2,2,2-trifluoroethyl)selanyl)ethan-1-amine (FSeN). 2,2'-

dislanedyldiethanamine dihydrochloride (500 mg), EtOH (10 mL), and NaOH solution (2 mL, 1.56 M) were added into a 50 mL pressure bottle and stirred for 10 min to obtain an orange solution. Then, NaBH₄ (118 mg) was added under nitrogen protection and stirred until the color faded. Finally, 2-iodo-1,1,1-trifluoroethane (600 μL) was injected into the bottle. The reaction mixture was sealed and heated at 50 °C for 3 h, followed by an additional 6 h treatment at 75 °C. The final reaction solution was mixed with saturated sodium chloride and extracted using dichloromethane. After the removal of the volatile components *via* rotary evaporation, a yellow liquid product was obtained with a yield of 58%.

Synthesis of 2-((2,2,2-trifluoroethyl)seleninyl)ethan-1-amine (FSeON). FSeN (aq., 30 mM) was mixed with H₂O₂ (30 mM) at 37 °C for 12 h to fully oxidize the FSeN. And then the unreacted H₂O₂ was removed to obtain 2-((2,2,2-trifluoroethyl)seleninyl)ethan-1-amine (FSeON). ¹H-NMR and ¹⁹F-NMR spectra at different pH of FSeON were recorded. Additionally, mass spectra of FSeON were recorded in the positive ion mode.

Synthesis of PIBAM-FSeN polymer. Poly(isobutylene-alt-maleic anhydride) (PIBAM, 181 mg) and 2-((2,2,2-trifluoroethyl)seleninyl)ethan-1-amine (FSeN, 206 mg) were dissolved in 2 mL of DMF under magnetic agitation. After stirring at room temperature for 48 h, the polymer (PIBAM-FSeN) was precipitated. Then, the precipitate was redissolved in THF and precipitated in hexane twice more for purification. After drying, 344 mg of yellow solid was obtained as the product (yield 89%).

Preparation of PIBAM-FSeN NPs. PIBAM-FSeN NPs were prepared by using the ultrasonic emulsification method. In brief, PIBAM-FSeN (50 mg) was dissolved into a mixture of DMF (200 μL) and CH₂Cl₂ (600 μL). The mixture was then added into a NaOH aqueous solution (12 mM, 10 mL), followed by ultrasonication treatment for 6 min (400 W, 3 s "on" and 3 s "off" in turn). The resultant emulsion was stirred for 2 h at 45 °C to remove CH₂Cl₂, yielding a clear solution. After undergoing multiple ultrafiltration, the PIBAM-FSeN NPs colloidal solution was collected for later use.

Preparation of PIBAM-FSeON NPs and semioxidized PIBAM-FSeN NPs. PIBAM-FSeON NPs and semioxidized PIBAM-FSeN NPs (the ratio of A_{Ox} -to- A_{Red} is 1:1) were obtained by full and partial oxidation of PIBAM-FSeN NPs with different amount of H₂O₂ as oxidant,

respectively. Before the oxidation, the concentration of PIBAM-FSeN NPs was quantified by ^{19}F NMR first. A standard curve was used to calculate the concentration of F atoms, and then the concentration of Se atoms could be calculated by equation (1).

$$C_{Se} = \frac{1}{3}C_F \quad \text{equation (1)}$$

1.1 eq. or 0.5 eq. of H_2O_2 was added into the aqueous solution of PIBAM-FSeN NPs to fully and partially transform the selenide ether into selenoxide, respectively. After incubating for 12 h at 37 °C, the unreacted H_2O_2 was removed by dialysis. The solution was collected for later use.

The reversible responsiveness in the presence of H_2O_2 and Na_2S . FSeN or PIBAM-FSeN NPs were mixed with different contents (0 - 1.0 eq.) of H_2O_2 and then incubated at 37 °C for 12 h, respectively. ^{19}F -NMR and ^{19}F -MRI were used to investigate the reaction results. To reversibly reduce the probe, FSeON or PIBAM-FSeON NPs were mixed with different contents of Na_2S (0 - 1.0 eq.). To measure the ability for multiple reversible responses in a redox environment, FSeN or PIBAM-FSeN NPs were mixed with 1.1 eq H_2O_2 or 1.1 eq Na_2S successively. ^{19}F -NMR and ^{19}F -MRI were used to investigate the reaction results. The following parameters were used during ^{19}F -MR imaging: RARE sequence, FA = 90°, TR = 1200 ms, TE = 22.52 ms, NEX = 22, TA = 9 min 36 s, Excitation pulse bandwidth = 500 Hz.

The selective response of nanoprobcs. Various components were chosen to assess the selective responsiveness of nanoprobcs, including protein (bovine serum albumin, BSA), common metal cations (Na^+ , K^+ , Ca^{2+} , Mg^{2+}), complex biological fluid environment (human serum), common oxidizing agents ($\cdot\text{OH}$, ONOO^- , $^1\text{O}_2$, ClO^- , H_2O_2) and reducing agents (Vc, L-Cys, GSH, Na_2S , DTT). $\cdot\text{OH}$ was generated by mixing aqueous solutions of H_2O_2 and Fe^{2+} in a 4:1 molar ratio. ONOO^- was produced by mixing aqueous solutions of H_2O_2 and NaNO_2 in an acid environment. In brief, the mixture of H_2O_2 (aq., 0.7 M, 1 mL) and HCl (aq., 0.6 M, 1 mL) was added into NaNO_2 (aq., 0.6 M, 1 mL) under rapid stirring. Then NaOH (aq., 1.5 M, 1 mL) was added to the above system to stabilize ONOO^- . The concentration of ONOO^- was determined by the absorption at 302 nm ($\epsilon = 1670 \text{ M}^{-1} \text{ cm}^{-1}$). $^1\text{O}_2$ was produced by mixing aqueous solutions of H_2O_2 and HClO in a 1:1 molar ratio.

Stability evaluation. The stability of PIBAM-FSeN NPs, PIBAM-FSeON NPs, and

semioxidized PIBAM-FSeN nanoprobe (the ratio of A_{Ox} -to- A_{Red} is 1:1) in water was assessed by measuring ^{19}F -NMR signals on multiple days. Additionally, the size of the nanoprobe was measured to evaluate their dimensional stability in water.

Cyclic voltammetry. Cyclic voltammetry (CV) measurements for semioxidized PIBAM-FSeN NPs (the ratio of A_{Ox} -to- A_{Red} is 1:1) were recorded to analyze the redox potentials. Experimental conditions are as follows. Electrolyte: 0.1 M KCl, pH = 6.50; working electrode: a glassy carbon electrode modified by semioxidized PIBAM-FSeN NPs; reference electrode: an Ag/AgCl electrode; counter electrode: a platinum wire. Scan rate: 0.05 V/s.

Measurement of pKa values of polymers. we measured the pKa values of polymers by pH titration according to previous literature.¹⁻³ In brief, the pH of the polymer solution (20 mg/mL, 2.0 mL) was adjusted to 4.5 by using 1.0 M HCl. Subsequently, 0.10 M NaOH was gradually added and the pH of the solution was measured using a FE28 pH Meter (Mettler Toledo). The buffering capacity at a pH value was calculated from the inverse slope of the titration curve as $\Delta(\text{NaOH})/\Delta\text{pH}$. The pKa is defined as the pH where a peak buffering capacity is.

Cytotoxicity evaluation. DC2.4 cells line was obtained from the Hunan Fenghui Biotechnology Co., Ltd (Changsha, China). DC2.4 cells were cultured in Dulbecco's Modified Eagle's Medium (DMEM) supplemented with 10% fetal bovine serum. All cells were maintained in a humidified atmosphere containing 5% CO_2 . Cytotoxicity was evaluated using 3-(4,5-dimethylthiazol-2-yl)-2,5-diphenyltetrazolium bromide (MTT) assays. Firstly, DC2.4 cells were seeded into a 96-well plate (1×10^4 cells/well) and incubated for 24 h. Then, they were treated with PIBAM-FSeN NPs, PIBAM-FSeON NPs, or semioxidized PIBAM-FSeN NPs (the ratio of A_{Ox} -to- A_{Red} is 1:1) at various concentrations for 24 h, respectively. Subsequently, a solution of MTT (5 mg/mL, 20 μL) was added to each well, and the cells were incubated for another 4 h at 37 °C. Finally, the media in each well was replaced with 100 μL of DMSO, and the absorbance at 492 nm of each well was measured on a microplate reader.

Animal model. All experiments involving animals were approved and performed in accordance with the guidelines of the Institutional Animal Care and Use Committee (IACUC) of the China-Japan Friendship Hospital and Beijing University of Chemical Technology. Five-week-old female Balb/c mice with an average weight of 15 g were provided by SPF Biotechnology Co.,

Ltd. 4T1 cells (2.0×10^6 cells) suspended in PBS (100 μ L) were subcutaneously injected into the right groin of each mouse. When the tumors reached approximately about 400 mm³, mice were used in the experiments. The tumor volumes were calculated using the following formula:

$$\text{The tumor volume} = \frac{1}{2} \times L \times \text{length} \times \text{Width}^2.$$

MR-imaging of redox status *in vivo*. To visualize the redox status in tumors, semioxidized PIBAM-FSeN NPs (the ratio of A_{Ox} -to- A_{Red} is 1:1) (140 mg/mL, 25 μ L) were injected into the tumors, and the same dose of semioxidized PIBAM-FSeN NPs was injected subcutaneously into the left groin of the mice. The ¹⁹F-MR images were recorded at 0.5 h and 4 h post-injection, respectively. *N*-acetyl cysteine (NAC) was used as a model drug to alter the redox status in tumors. After injecting semioxidized PIBAM-FSeN NPs (the ratio of A_{Ox} -to- A_{Red} is 1:1) in the tumor, NAC (0.1 M, 100 μ L) was paratumoral injected at 4 h. The ¹⁹F-MR images were recorded at 1 h, 3 h and 6 h after the injection of nanoprobe. The following parameters were used during ¹⁹F-MR imaging: RARE sequence, FA = 90°, TR = 1200 ms, TE = 22.52 ms, NEX = 22, TA = 9 min 36 s, Excitation pulse bandwidth = 500 Hz. The RF pulses were selected on the ¹⁹F-NMR peak at -58.7 ppm for imaging in the oxidation channel and selected on the ¹⁹F NMR peak at -64.2 ppm for imaging in the reduction channel. Ratio images were obtained by ImageJ software.

Biosafety assessment. Seven-week-old female BABL/c mice were i.v. injection of PBS or semioxidized PIBAM-FSeN NPs (75 mg/mL, 25 μ L). The serums and major organs were collected after 7 days. H&E staining of major organs and biochemistry analysis of serums were checked to evaluate the biosafety of this nanoprobe.

Linear-regression analysis. Linear regression analysis was performed using origin software. A statistical significance analysis (t test) was performed for the intercepts, when assume the intercepts were 0 (for PIBAM-FSeN NPs), 0.5000 (for semioxidized PIBAM-FSeN NPs) or 1.0 (for PIBAM-FSeON NPs), the significant level was set at 0.05. If no significance was observed, the intercept was fixed as 0 (for PIBAM-FSeN NPs), 0.5000 (for semioxidized PIBAM-FSeN NPs) or 1.0 (for PIBAM-FSeON NPs) and the slopes was recalculated.

2. Supplemental Figures and Tables

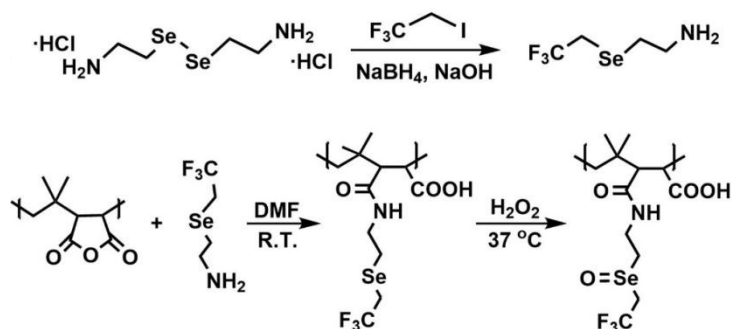


Figure S1. Synthetic scheme of FSeN, PIBAM-FSeN and PIBAM-FSeON.

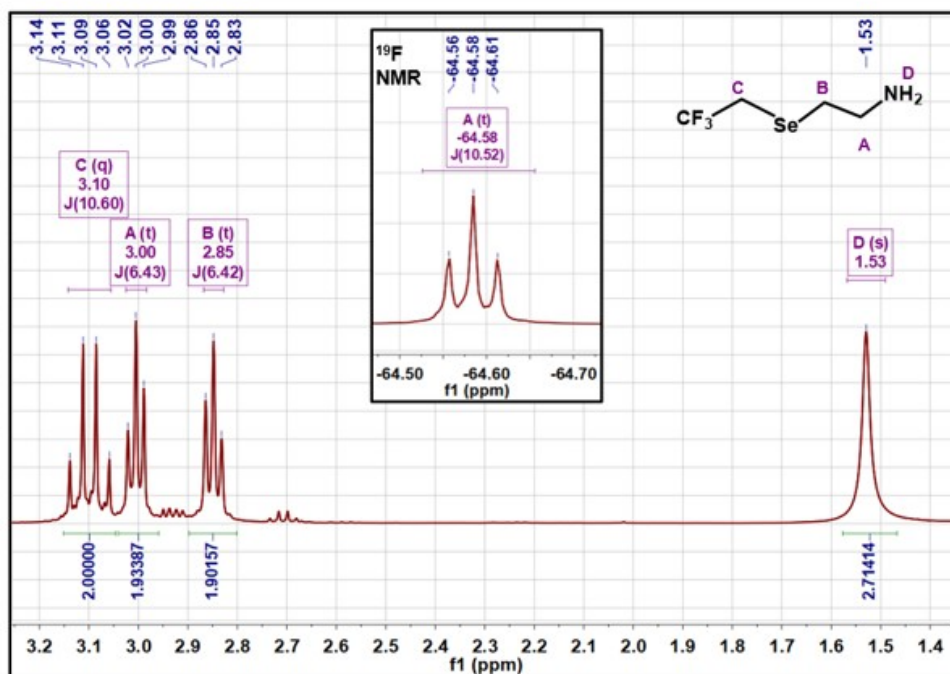


Figure S2. ^1H -NMR and ^{19}F -NMR spectra of 2-((2,2,2-trifluoroethyl)selanyl)ethan-1-amine (FSeN) in CDCl_3 . ^1H -NMR (400 MHz, CDCl_3): $\delta = 3.1$ (2H, q, $J = 10.60$ Hz, CF_3CH_2), 3.00 (2H, t, $J = 6.43$ Hz, SeCH_2CH_2), 2.86 (2H, t, $J = 6.42$ Hz, SeCH_2CH_2) ppm. ^{19}F -NMR (376 MHz, CDCl_3): $\delta = -64.6$ (t, $J = 10.52$ Hz) ppm.

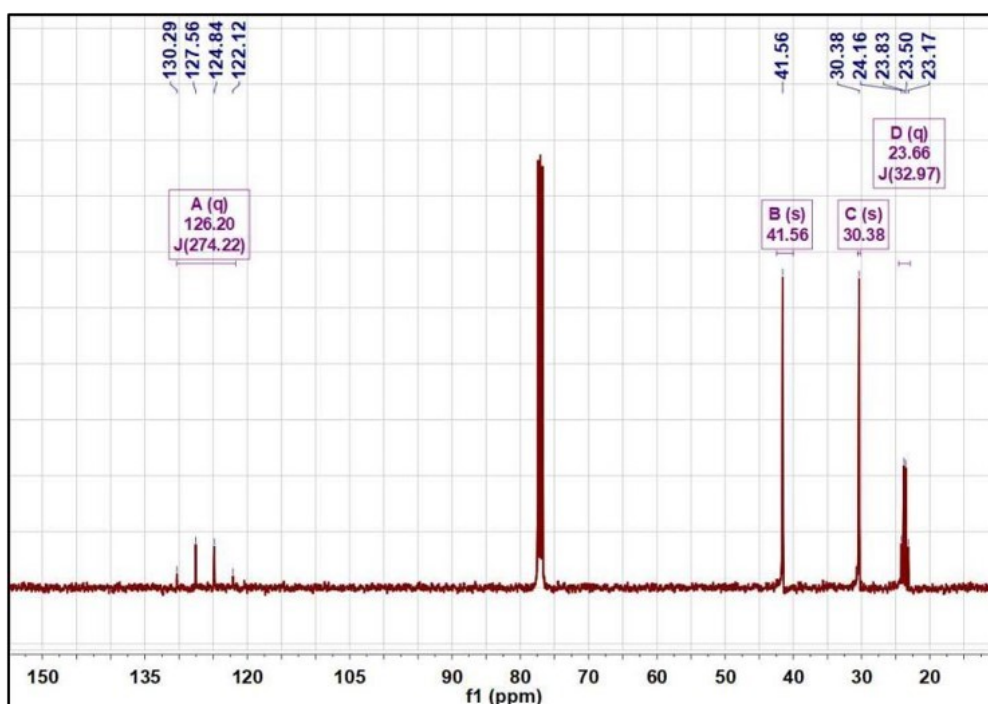


Figure S3. ^{13}C -NMR spectra of 2-((2,2,2-trifluoroethyl)selanyl)ethan-1-amine (FSeN) in CDCl_3 . ^{13}C -NMR (100 MHz, CDCl_3): $\delta = 126.20$ (q, $J = 274.22$ Hz), 41.56 (s), 30.38 (s), 23.66 (q, $J = 32.97$ Hz) ppm.

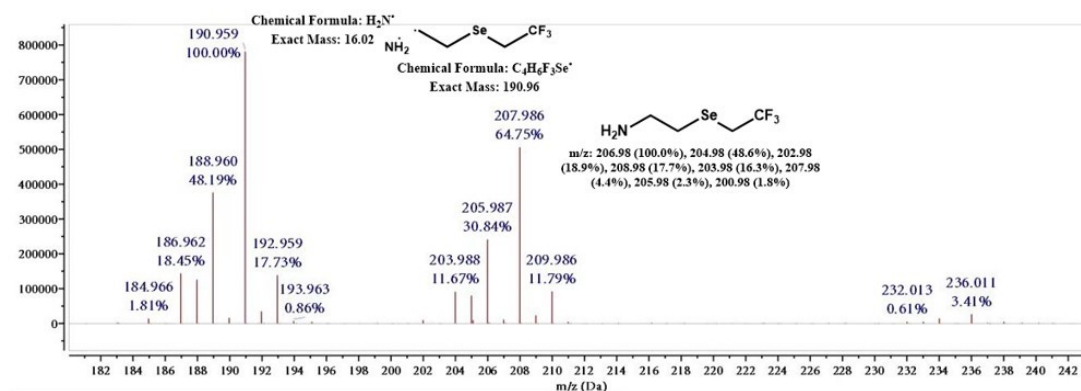


Figure S4. Mass spectra of 2-((2,2,2-trifluoroethyl)selanyl)ethan-1-amine (FSeN). ESI-MS m/z : calculated for $\text{C}_4\text{H}_8\text{F}_3\text{NSe}$ ($\text{M} + \text{H}^+$), 207.98; found: 207.986. The distribution of isotopic peaks reveals the presence of selenium. Due to the breaking of the amino group, a peak at 190.959 was also found for $\text{C}_4\text{H}_7\text{F}_3\text{Se}^+$ ($\text{M} + \text{H}^+$), calculated: 190.96; found: 190.959.

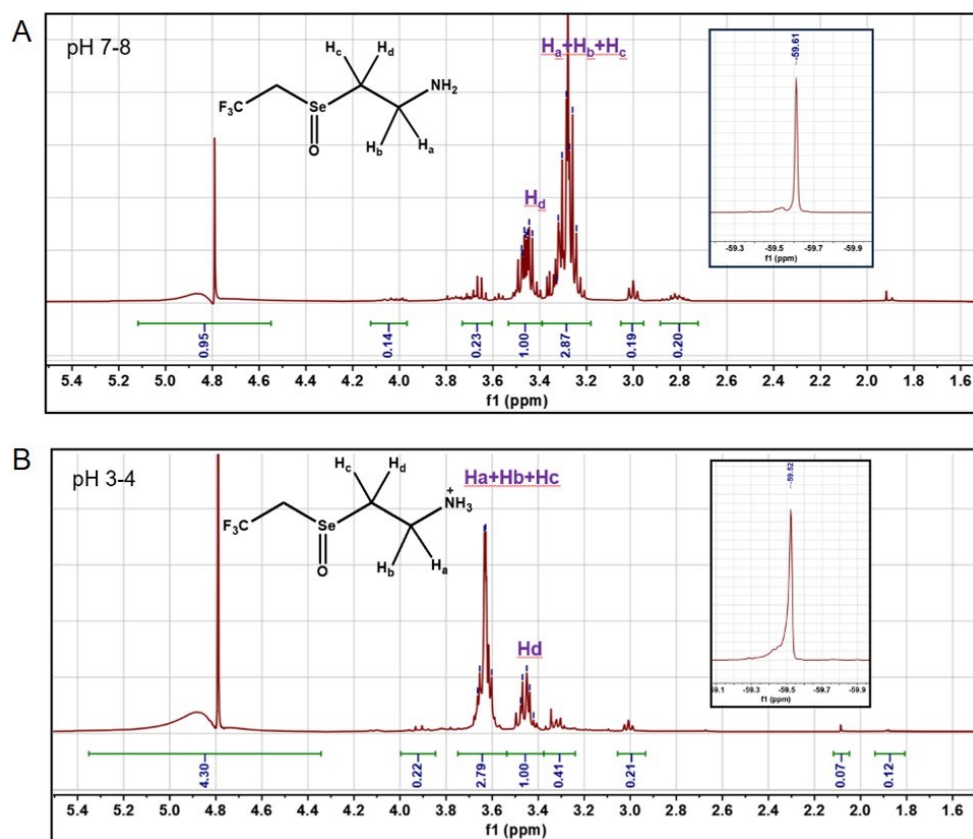


Figure S5. ^1H and ^{19}F -NMR spectra of 2-((2,2,2-trifluoroethyl)seleninyl)ethan-1-amine (FSeON) in D_2O at different pH. ^1H -NMR for FSeON (400 MHz, D_2O , pH 7-8): $\delta = 3.27$ (3H, m, $\text{H}_a+\text{H}_b+\text{H}_c$), 3.45 (1H, m, H_d) ppm. ^1H -NMR of FSeON (400 MHz, D_2O , pH 3-4): $\delta = 3.63$ (3H, m, $\text{H}_a+\text{H}_b+\text{H}_c$), 3.45 (1H, m, H_d) ppm. ^{19}F -NMR for FSeON (376 MHz, D_2O , pH 7-8): $\delta = -59.6$ ppm. ^{19}F -NMR for FSeON (376 MHz, D_2O , pH 3-4): $\delta = -59.5$ ppm. The H atoms between selenoxide and trifluoromethyl disappeared in the ^1H spectra, indicating they became reactive hydrogens attributed to the strong electron absorption effect of selenoxide and trifluoromethyl. In an acid environment, the chemical shift of $\text{H}_a+\text{H}_b+\text{H}_c$ was moved downfield, indicating the protonation of amino, which means the amino group remains after the oxidation process.

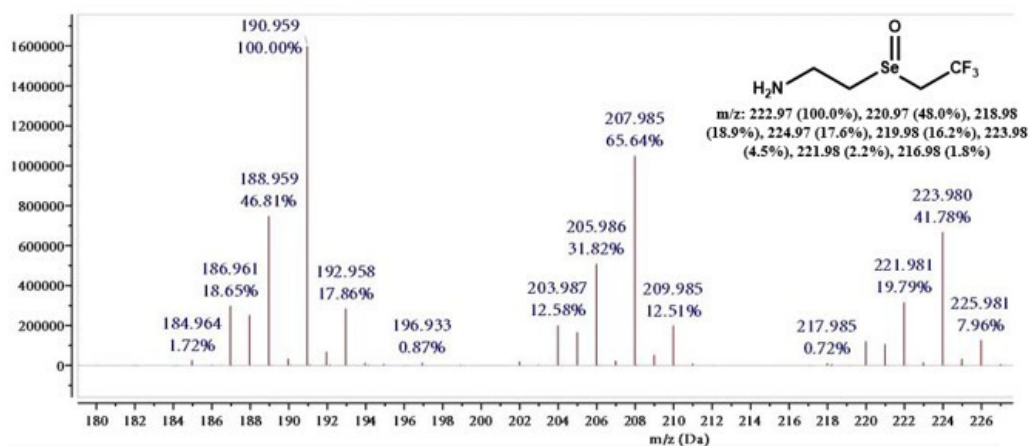


Figure S6. Mass spectra of 2-((2,2,2-trifluoroethyl)seleninyl)ethan-1-amine (FSeON). ESI-MS m/z: calculated for $C_4H_8F_3NOSe$ ($M + H^+$), 223.97, found: 223.980. A molecular ion peak at 223.97 ($207.98 + 16$) for $C_4H_8F_3NOSe$ ($M + H^+$) was detected, indicating that the selenide ether was oxidized to selenoxide.

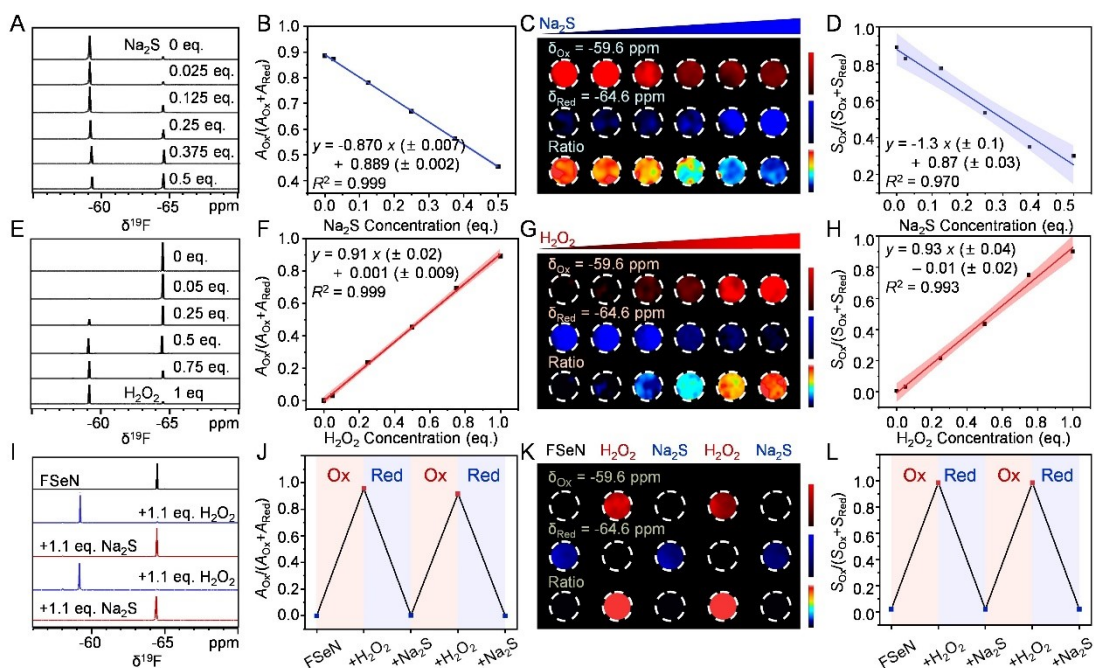


Figure S7. *In vitro* response behavior of FSeN and FSeON molecules. (A) Evolution of ^{19}F -NMR spectra, (B) the integral proportion of Ox-peak area [$A_{\text{Ox}}/(A_{\text{Ox}} + A_{\text{Red}})$] in ^{19}F -NMR spectra, (C) ^{19}F -MR images in Ox-, Red-channel, and corresponding $S_{\text{Ox}}/(S_{\text{Ox}}+S_{\text{Red}})$ -channel, and (D) the ^{19}F -MRI signal ratio of $S_{\text{Ox}}/(S_{\text{Ox}}+S_{\text{Red}})$ on the solution of FSeON molecule (90 mM) mixed with Na_2S (0.025-0.5 eq). The band in the graph is the 95% confidence interval band. (E) Evolution of ^{19}F -NMR spectra, (F) the integral proportion of Ox-peak area [$A_{\text{Ox}}/(A_{\text{Ox}} + A_{\text{Red}})$] in ^{19}F -NMR spectra, (G) ^{19}F -MR images in Ox-, Red-channel, and corresponding $S_{\text{Ox}}/(S_{\text{Ox}}+S_{\text{Red}})$ -channel, and (H) the ^{19}F -MRI signal ratio of $S_{\text{Ox}}/(S_{\text{Ox}}+S_{\text{Red}})$ on the solution of FSeN molecule (90 mM) treated with H_2O_2 (0.05-1 eq). The band in the graph is the 95% confidence interval band. (I) Evolution of ^{19}F -NMR spectra, (J) the integral proportion of Ox-peak area [$A_{\text{Ox}}/(A_{\text{Ox}} + A_{\text{Red}})$] in ^{19}F -NMR, (K) ^{19}F -MR images in ox-, re-channel, and corresponding ratio-channel, (L) the ^{19}F -MRI ratio of $S_{\text{Ox}}/(S_{\text{Ox}}+S_{\text{Red}})$ on the solution of FSeN molecule (90 mM) treated with H_2O_2 (1.1 eq.) and Na_2S (1.1 eq.) in succession. A_{Ox} and A_{Red} refer to the ^{19}F -NMR peak area at 59.6 ppm (oxidation state) and 64.6 ppm (reduction state), respectively. Meanwhile, S_{Ox} and S_{Red} refer to the ^{19}F -MRI signal intensity at 59.5 ppm (oxidation state) and 64.6 ppm (reduction state), respectively.

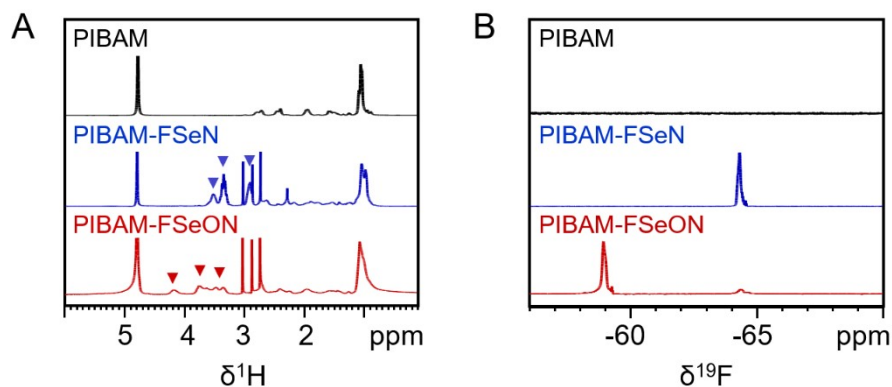


Figure S8. $^1\text{H-NMR}$ (A) and $^{19}\text{F-NMR}$ (B) spectra of PIBAM (black line), PIBAM-FSeN (blue line) and PIBAM-FSeON (red line) in D_2O .

In **Figure S8A**, the blue arrows indicate the characteristic peaks of the H atoms next to the selenide ether, and the red arrows indicate the characteristic peaks of the H atoms next to the selenoxide. An apparent low field shift was found because of the decreased shielding effects after the oxidation of selenide ether. In **Figure S8B**, no $^{19}\text{F-NMR}$ signal was observed in PIBAM. After being modified with FSeN, a distinct peak appeared at -64.2 ppm in PIBAM-FSeN. An obvious low field shift (shift to -58.7 ppm) was found in PIBAM-FSeON because of the decreased shielding effects along with the oxidation of selenide ether, which is consistent with the phenomenon in $^1\text{H-NMR}$ spectra.

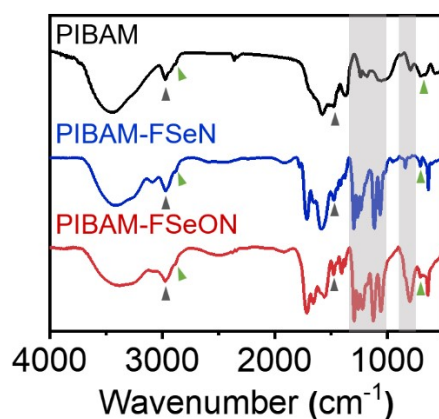


Figure S9. IR spectra of PIBAM (black line), PIBAM-FSeN (blue line) and PIBAM-FSeON (red line).

As shown in **Figure S9**, the characteristic peaks of carboxyl, methyl and methylene in the backbone were observed in three polymers. The peaks around 3400 cm^{-1} belong to the stretching vibration of O-H. The peaks at 2973 , 1470 , and 1374 cm^{-1} are attributed to the vibration of C-H in methyl, and the peaks at 2875 and 712 cm^{-1} are attributed to the vibration of C-H in methylene. After modification with FSeN, prominent stretching vibration peaks of trifluoromethyl and selenide ether appeared at $1000\text{-}1300\text{ cm}^{-1}$, indicating the successful grafting of FSeN to form the PIBAM-FSeN. After oxidation treatment with H_2O_2 , a peak around 800 cm^{-1} in PIBAM-FSeON was assigned to the characteristic peak of selenoxide,⁴ indicating the successful conversion from selenide ether to selenoxide.

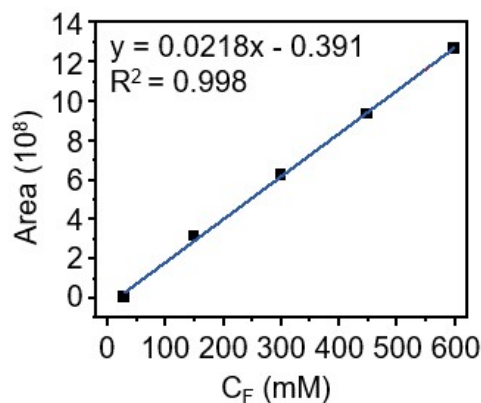


Figure S10. The plot of the ^{19}F -NMR integral area versus ^{19}F concentration (C_F/mM).

The ^{19}F -NMR integral area of the PIBAM-FSeN (500 μL , 20.0 mg/mL) was 3.40×10^8 .

$$C_F = \frac{3.40 \times 10^8 + 3.91 \times 10^7}{2.18 \times 10^6} = 174 \text{ mM}$$

$$m = 174 \text{ mM} \times 500 \mu\text{L} \times 19.0 \frac{\text{g}}{\text{mol}} = 1.65 \text{ mg}$$

$$W_F = \frac{1.65 \text{ mg}}{500 \mu\text{L} \times 20 \text{ mg/mL}} = 16 \%$$

The ^{19}F NMR integral area of PIBAM-FSeON (400 μL , 25.0 mg/mL) was 4.01×10^8 .

$$C_F = \frac{4.01 \times 10^8 + 3.91 \times 10^7}{2.18 \times 10^6} = 202 \text{ mM}$$

$$m = 202 \text{ mM} \times 400 \mu\text{L} \times 19.0 \frac{\text{g}}{\text{mol}} = 1.53 \text{ mg}$$

$$W_F = \frac{1.53 \text{ mg}}{400 \mu\text{L} \times 25 \text{ mg/mL}} = 15 \%$$

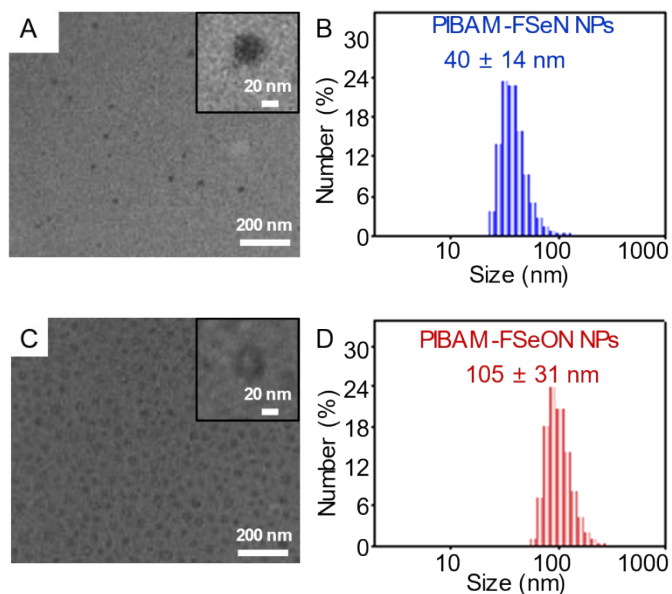


Figure S11. TEM image (A and C) and the DLS size distribution (B and D) of PIBAM-FSeN NPs (A and B) and PIBAM-FSeON NPs (C and D), respectively. The concentration of probes for DLS measurement are 10 mg/mL (in H₂O).

The self-assembly behavior of polymers in water was investigated. The obtained PIBAM-FSeN NPs and PIBAM-FSeON NPs were assessed by transmission electron microscopy (TEM, **Figure S11A** and **S11C**) and dynamic light scattering (DLS, **Figure S11B** and **S11D**), exhibiting good size distribution with an average diameter of 40 ± 14 nm and 105 ± 31 nm, respectively. After oxidation, the particle size was obviously increased, which is 2.6 times that of PIBAM-FSeN NPs due to the good hydrophilicity of selenoxide.

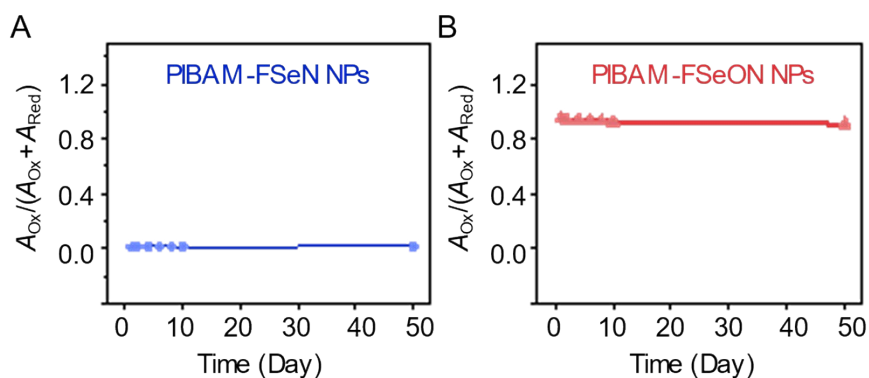


Figure S12. The stability tests of ^{19}F -NMR signal on PIBAM-FSeN NPs (A) and PIBAM-FSeON NPs (B) dispersed in water. (n=3, error bars represent standard deviation (SD)).

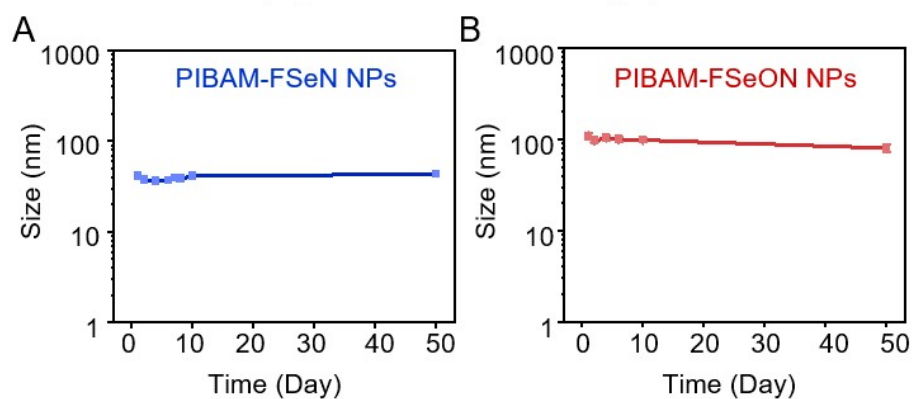


Figure S13. The stability tests of DLS size distribution on PIBAM-FSeN NPs (A) and PIBAM-FSeON NPs (B) dispersed in water. (n=3, error bars represent standard deviation (SD)).

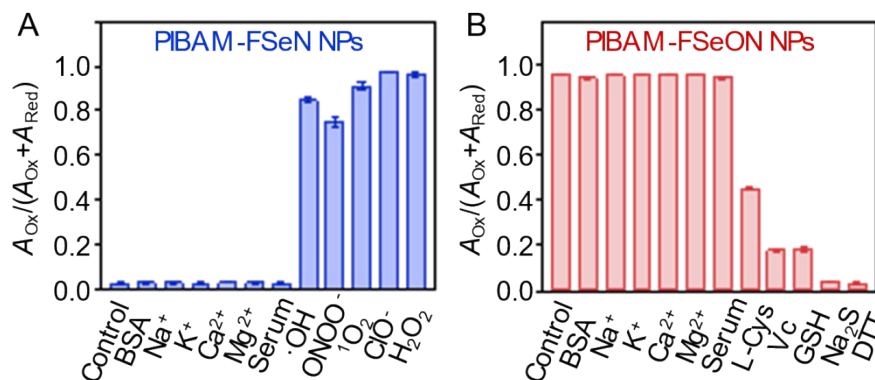


Figure S14. The selective response of PIBAM-FSeN (A) and PIBAM-FSeON (B) NPs to different analytes. The concentration of the probes was 15 mM, and the molar ratio of the probe and the analyte was 1:1. (n=3, error bars represent standard deviation (SD)).

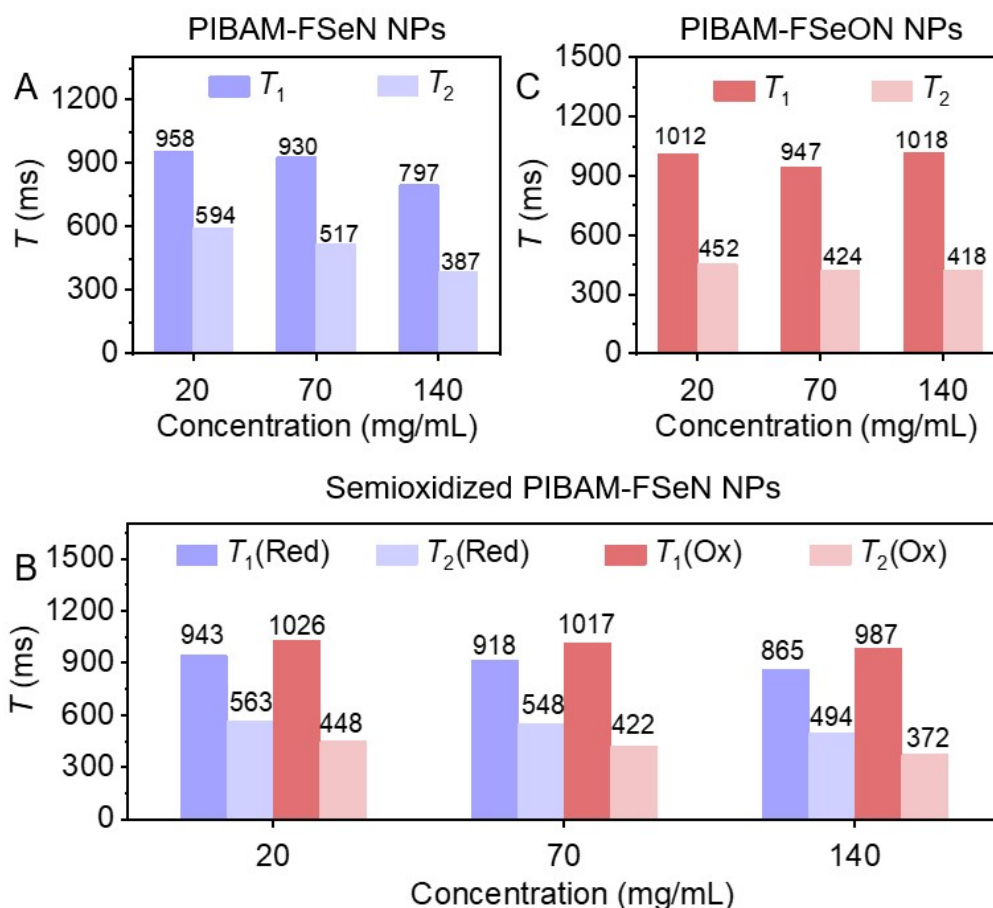


Figure S15. The T_1 and T_2 relaxation time of PIBAM-FSeN NPs (A), semioxidized PIBAM-FSeN NPs (B) and PIBAM-FSeON NPs (C) at different concentrations (in water).

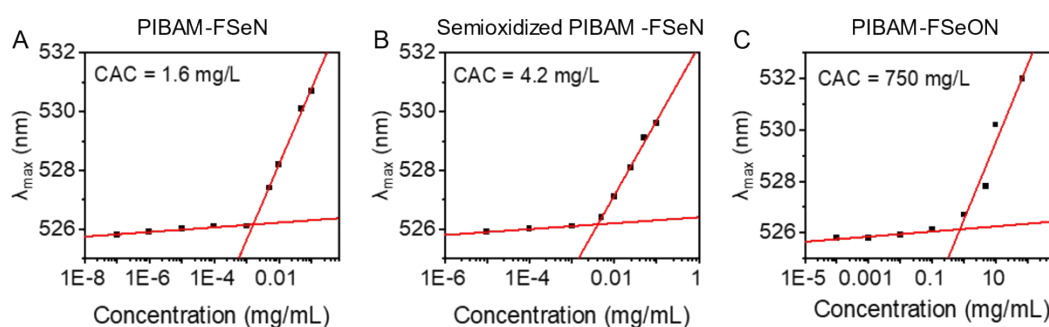


Figure S16. The critical aggregation concentration (CAC) determined by maximum absorption wavelength from Rhodamine 6G as a function of concentration of PIBAM-FSeN polymer (A), semioxidized PIBAM-FSeN polymer (B) and PIBAM-FSeON polymer (C).

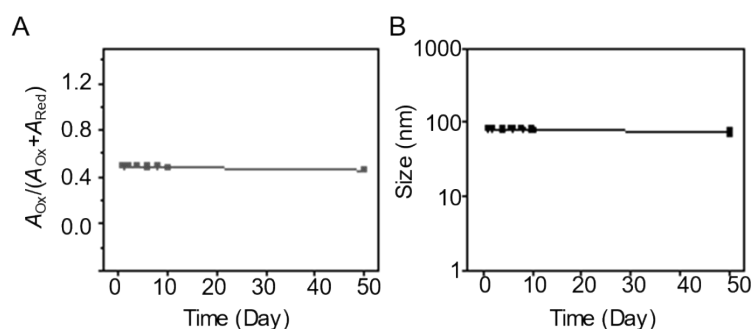


Figure S17. The stability of ^{19}F -NMR signal (A) and DLS size distribution (B) on semioxidized PIBAM-FSeN nanoprobes (the ratio of A_{Ox} -to- A_{Red} is 1:1) dispersed in water. ($n=3$, error bars represent standard deviation (SD)).

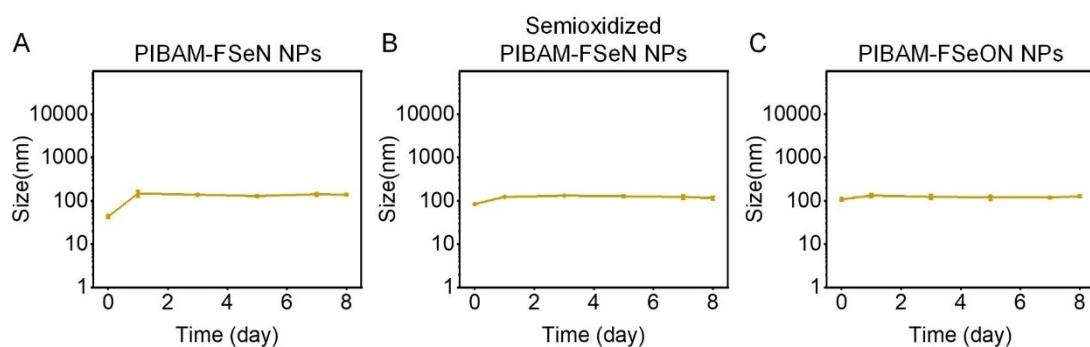


Figure S18. The stability of DLS size distribution on PIBAM-FSeN (A), semioxidized PIBAM-FSeN NPs (B) and PIBAM-FSeON NPs (C) dispersed in bovine serum albumin (BSA) solution (2 mg/mL). ($n=3$, error bars represent standard deviation (SD)).

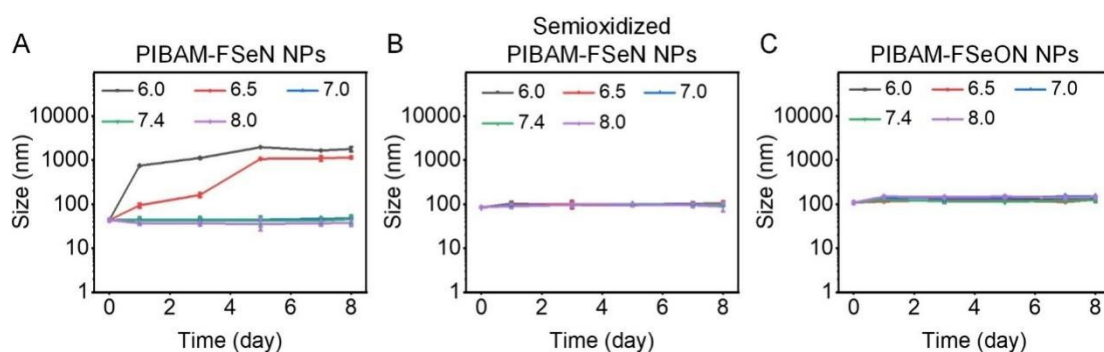


Figure S19. The stability of the probe size for PIBAM-FSeN NPs (A), semioxidized PIBAM-FSeN NPs (B) and PIBAM-FSeON NPs (C) at different pH (0.2 M PB buffer, pH = 6.0, 6.5, 7.0, 7.4 and 8.0). ($n=3$, error bars represent standard deviation (SD)).

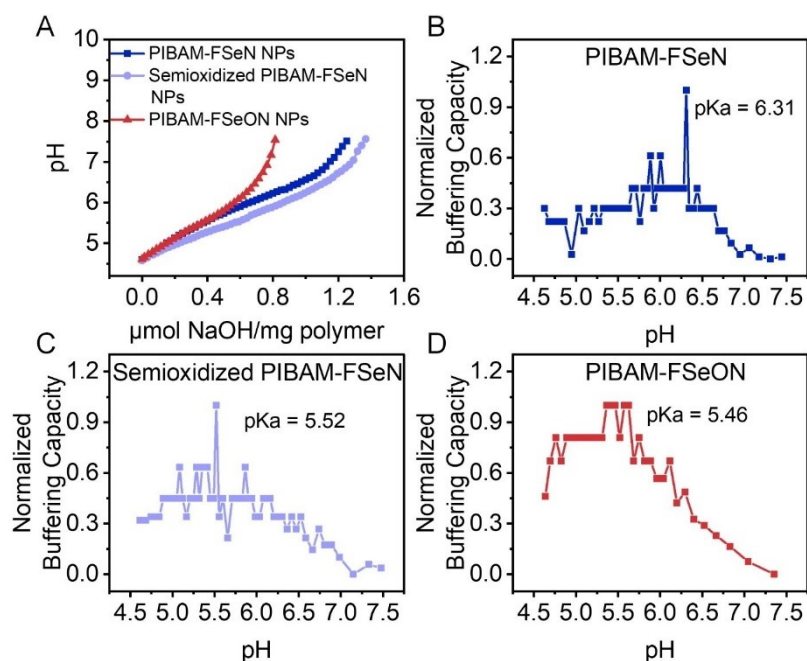


Figure 20. (A) Titration curve of PIBAM-FSeN, Semioxidized PIBAM-FSeN and PIBAM-FSeON in the pH range (4.5-7.5). The normalized buffering capacity of PIBAM-FSeN (B), semioxidized PIBAM-FSeN (C) and PIBAM-FSeON (D) at different pH value, buffering capacity at a pH value was calculated from the inverse slope of the titration curve as $\Delta(\text{NaOH})/\Delta\text{pH}$.

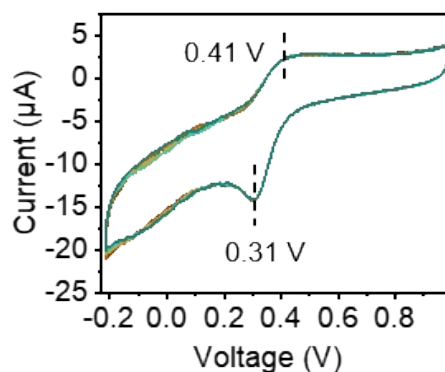


Figure S21. The cyclic voltammogram of semioxidized PIBAM-FSeN nanoprobe (the ratio of A_{Ox} -to- A_{Red} is 1:1) measured five times continuously. Electrolyte: 0.1 M KCl, pH = 6.50; working electrode: a glassy carbon electrode modified by semioxidized nanoprobe; reference electrode: an Ag/AgCl electrode; counter electrode: a platinum wire. Scan rate: 0.05 V/s.

As shown in **Figure S21**, the probe could be oxidized at 0.41 V and reduced at 0.31 V. According to **Table S2** and **Table S3**, the redox potentials of common oxidizing substances (H_2O_2 , ClO^- , $^1\text{O}_2$, ONOO^- and $\cdot\text{OH}$) were all exceed the oxidation potential of this nanoprobe and the redox potentials of common reduction substances (DTT, H_2S , GSH, L-Cys and Vc) were all below the reduction potential of this nanoprobe, which means the possibility of the redox reactions when the probe meets these substances. This result is consistent with **Figure 3E**. The curve was stable in five cycles, indicating the reaction can occur cyclically and stably.

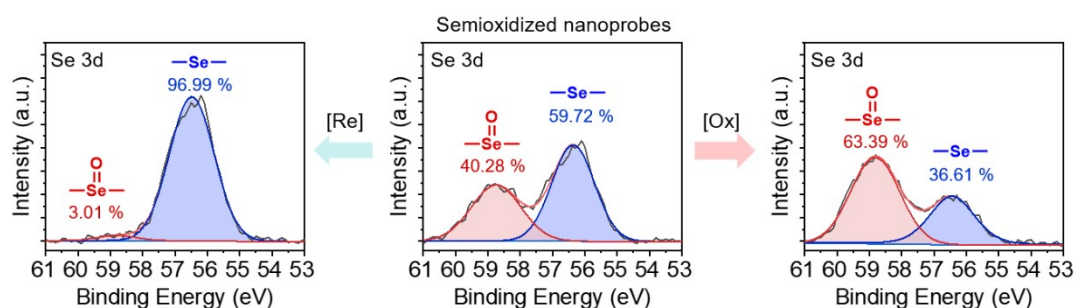


Figure S22. XPS spectra of Se in the semioxidized PIBAM-FSeN nanoprobe (the ratio of A_{Ox} -to- A_{Red} is 1:1) before and after reacting with reduction or oxidation substances.

As shown in **Figure S22**, the redox capacity of semioxidized nanoprobe was proved by XPS. In the XPS spectra of semioxidized nanoprobe, two peaks were recorded clearly, which belong to selenide ether (56.4 eV) and selenoxide (58.7 eV), respectively.⁵⁻⁷ When meets reduction substances, such as Na_2S , part of the selenoxide in the probe could be converted to selenide ether, along with the descending integral area of the peak at 58.7 eV and the ascending integral area of the peak at 56.4 eV. An opposite phenomenon was found when the probe met oxidation substances like H_2O_2 . This result demonstrates the effectivity of the response groups in the probe, which is conducive to the development of subsequent biological applications.

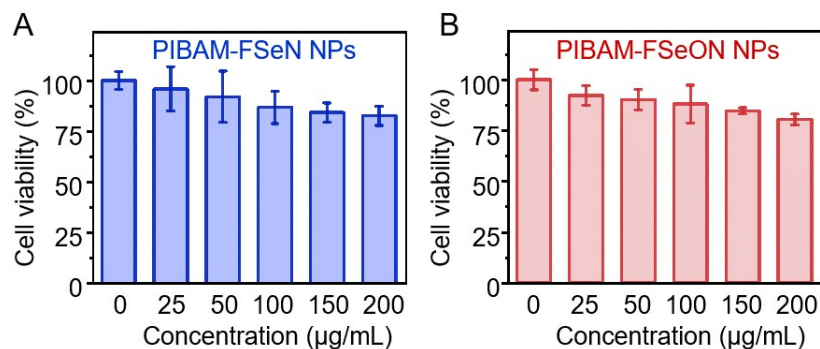


Figure S23. The cytotoxicity of PIBAM-FSeN (A) and PIBAM-FSeON NPs (B) on DC2.4 cells. (n=5, error bars represent standard deviation (SD)).

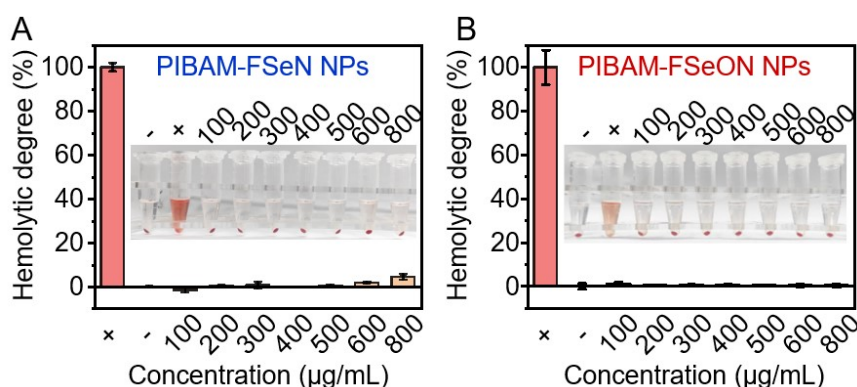


Figure S24. The results of hemolysis tests on PIBAM-FSeN (A) and PIBAM-FSeON (B) NPs. (n=3, error bars represent standard deviation (SD)).

Figure S23 demonstrates that even after incubation with PIBAM-FSeON NPs and PIBAM-FSeN NPs at a high concentration of 200 µg/mL for 24 h, the DC2.4 cells maintained a viability of over 80%. Then, the hemolysis tests (**Figure S24**) indicated that the PIBAM-FSeON NPs and PIBAM-FSeN NPs exhibited a hemolytic ratio below 5%, even at a concentration of 800 µg/mL. All the results suggest good biocompatibility.

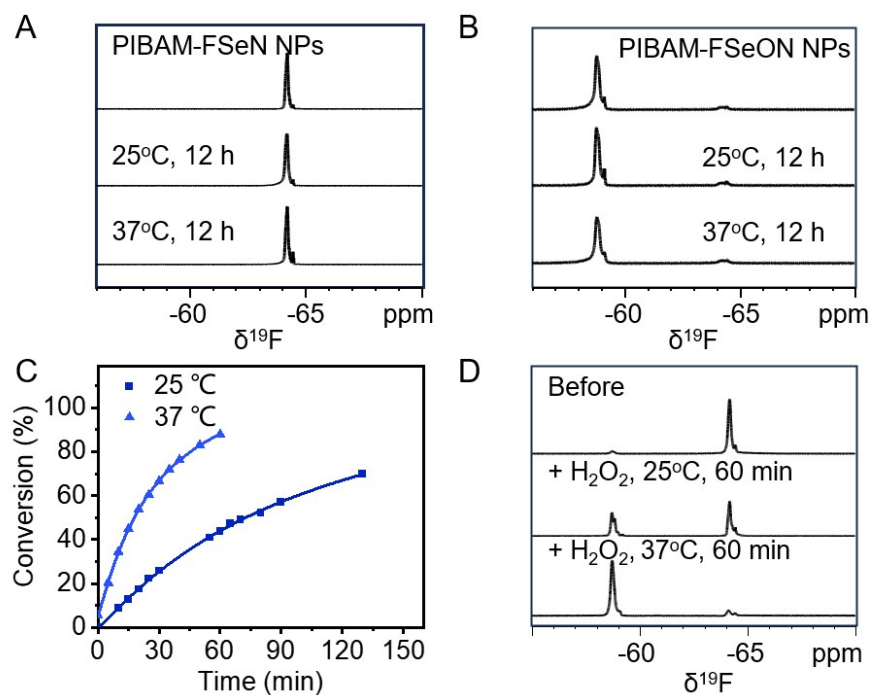


Figure S25. (A-B) The ^{19}F -NMR spectra of PIBAM-FSeN and PIBAM-FSeON NPs (30 mM) at different temperatures. (C) The conversion rate of selenide ether to selenoxide at different temperatures. The molar ratio of PIBAM-FSeN NPs and oxidant (H_2O_2) was 1:1. (D) The corresponding ^{19}F -NMR spectra of the solution shown in **Figure S25C** at 60 min.

As shown in **Figure S25**, the ^{19}F -NMR signals of PIBAM-FSeN and PIBAM-FSeON NPs were constant at both 25 °C and 37 °C, implying their good stability. When 1 eq. of H_2O_2 was added to the PIBAM-FSeN colloid solution, the oxidation reaction proceeded quickly. The reaction completed over 80% among 60 min at 37 °C, which is potential for *in vivo* imaging.

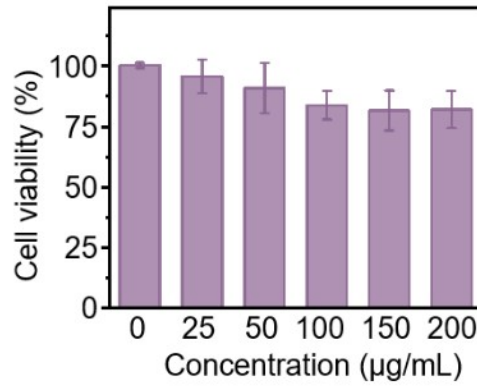


Figure S26. The cytotoxicity of semioxidized PIBAM-FSeN nanoprobe on DC2.4 cells. (n=5, error bars represent standard deviation (SD)).

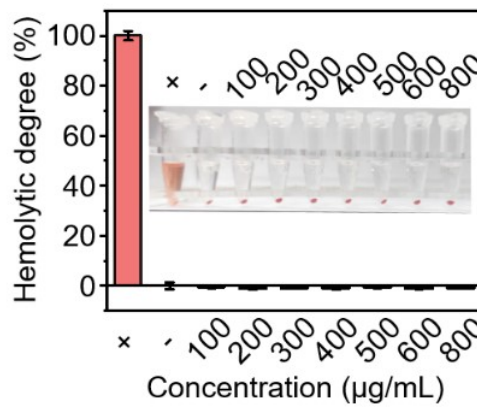


Figure S27. The results of hemolysis tests on semioxidized PIBAM-FSeN nanoprobe. (n=3, error bars represent standard deviation (SD)).

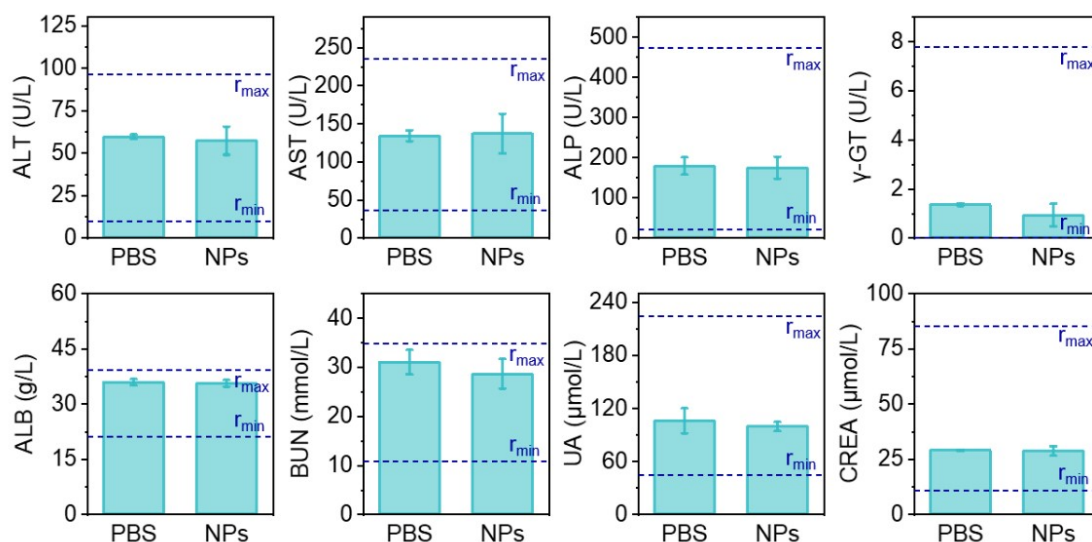


Figure S28. Biochemistry analysis of female BABL/c mice at 7 days post i.v. injection of semioxidized PIBAM-FSeN nanoprobes (70 mg/mL, 25 μ L). ALT, alanine aminotransferase; AST, glutamic oxaloacetic transaminase; ALP, alkaline phosphatase; γ -GT, gamma-glutamyltransferase; ALB, albumin; BUN, blood urea nitrogen; UA, uric acid; CREA, creatinine. The Blue dotted line indicates the normal reference values (r_{\min} \rightarrow r_{\max}) for the mouse. No significant differences were detected, $n = 3$, error bars represent standard deviation (SD).

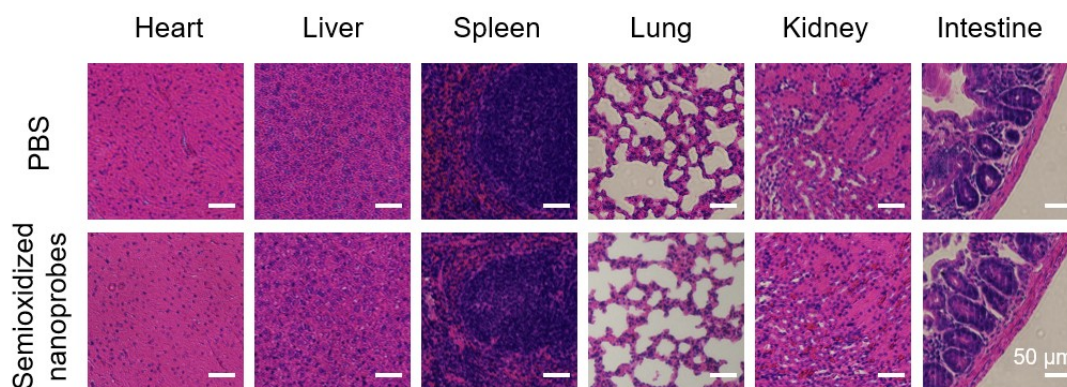


Figure S29. Representative H&E staining of dissected main organs from the female BABL/c mice at 7 days post i.v. injection of semioxidized PIBAM-FSeN nanoprobres (70 mg/mL, 25 μ L).

The blood biochemical analysis (**Figure S28**) of mice 7-day post-injection (i.v.) confirmed that no significant cytotoxicity was induced by the semioxidized PIBAM-FSeN nanoprobres. Additionally, histological hematoxylin and eosin (H&E) staining (**Figure S29**) further confirmed that no apparent pathological damage was caused to the major organs (heart, liver, spleen, lungs, kidneys, and intestines), indicating the excellent biocompatibility for *in vivo* biomedical applications.

Table S1. Relaxation property of FSeN molecule, FSeON molecule, PIBAM-FSeN, semioxidized PIBAM-FSeN and PIBAM-FSeON NPs

Samples	T_1 (s)	T_2 (s)	T_2/T_1
PIBAM-FSeN NPs ^a	0.96	0.59	0.62
PIBAM-FSeON NPs ^a	1.01	0.45	0.45
Semioxidized PIBAM-FSeN NPs ^a	0.94	0.56	0.60
(Peak _{Red} at -64.2 ppm)			
Semioxidized PIBAM-FSeN NPs ^a	1.03	0.45	0.44
(Peak _{Ox} at -58.7 ppm)			
FSeN molecule ^b	2.43	2.04	0.84
FSeON molecule ^b	1.82	1.47	0.80

^a Concentration of probe is 20 mg/mL; ^b Concentration of probe is 60 mM.










Table S2. The redox potentials of H₂O₂, ClO⁻, ¹O₂, ONOO⁻ and ·OH

Substances	H ₂ O ₂	ClO ⁻	¹ O ₂	ONOO ⁻	·OH
Redox potentials (V)	1.76	1.2	2.2	1.4	2.73
References	Ref-8	Ref-9	Ref-10	Ref-11	Ref-12

Table S3. The redox potentials of DTT, H₂S, GSH, L-Cys and Vc

Substances	DTT	H ₂ S	GSH	L-Cys	Vc
Redox potentials (V)	-0.33	-0.28	-0.24	-0.22	+0.08
References	Ref-13	Ref-14	Ref-15, Ref-16	Ref-15	Ref-15

Table S4. The photos of PIBAM-FSeN NPs, semioxidized PIBAM-FSeN NPs and PIBAM-FSeON NPs at different concentrations.

Samples	20 mg/mL	70 mg/mL	140 mg/mL
PIBAM-FSeN NPs			
Semioxidized PIBAM-FSeN NPs			
PIBAM-FSeON NPs			

3. Reference

- 1 F. Hausig, F. H. Sobotta, F. Richter, D. O. Harz, A. Traeger and J. C. Brendel, Correlation between Protonation of Tailor-Made Polypiperazines and Endosomal Escape for Cytosolic Protein Delivery, *ACS Applied Materials & Interfaces*, 2021, **13**, 35233-35247.
- 2 D. Routkevitch, D. Sudhakar, M. Conge, M. Varanasi, S. Y. Tzeng, D. R. Wilson and J. J. Green, Efficiency of Cytosolic Delivery with Poly(β -amino ester) Nanoparticles is Dependent on the Effective pKa of the Polymer, *ACS Biomaterials Science & Engineering*, 2020, **6**, 3411-3421.
- 3 D. R. Wilson, Y. Rui, K. Siddiq, D. Routkevitch and J. J. Green, Differentially Branched Ester Amine Quadpolymers with Amphiphilic and pH-Sensitive Properties for Efficient Plasmid DNA Delivery, *Molecular Pharmaceutics*, 2019, **16**, 655-668.

- 4 L. Yu, H.-L. Ke, F.-S. Du and Z.-C. Li, Redox-Responsive Fluorescent Polycarbonates Based on Selenide for Chemotherapy of Triple-Negative Breast Cancer, *Biomacromolecules*, 2019, **20**, 2809-2820.
- 5 Q. Li, K. L. Ng, X. Pan and J. Zhu, Synthesis of High Refractive Index Polymer with Pendent Selenium-Containing Maleimide and Use As a Redox Sensor, *Polym. Chem.*, 2019, **10**, 4279-4286.
- 6 Q. Li, S. Liu, M. Xu, X. Pan, N. Li, J. Zhu and X. Zhu, Selenide-Containing Soluble Polyimides: High Refractive Index and Redox Responsiveness, *Eur. Polym. J.*, 2020, **122**, 109358.
- 7 Z. Li, Y. Shang, L. Liu, H. Long, Y. Feng, L. Billon and H. Yin, Selenium-Decorated Biocompatible Honeycomb Films with Redox-Switchable Surface for Controlling Cell Adhesion/Detachment, *J. Colloid Interface Sci.*, 2023, **635**, 503-513.
- 8 E. Sitta, A. M. Gómez-Marín, A. Aldaz and J. M. Feliu, Electrocatalysis of H₂O₂ Reduction/Oxidation at Model Platinum Surfaces, *Electrochem. Commun.*, 2013, **33**, 39-42.
- 9 D. Oushiki, H. Kojima, T. Terai, M. Arita, K. Hanaoka, Y. Urano and T. Nagano, Development and Application of a Near-Infrared Fluorescence Probe for Oxidative Stress Based on Differential Reactivity of Linked Cyanine Dyes, *J. Am. Chem. Soc.*, 2010, **132**, 2795-2801.
- 10 Q. Yi, J. Ji, B. Shen, C. Dong, J. Liu, J. Zhang and M. Xing, Singlet Oxygen Triggered by Superoxide Radicals in a Molybdenum Cocatalytic Fenton Reaction with Enhanced REDOX Activity in the Environment, *Environ. Sci. Technol.*, 2019, **53**, 9725-9733.
- 11 R. Radi, Peroxynitrite, a Stealthy Biological Oxidant, *J. Biol. Chem.*, 2013, **288**, 26464-26472.
- 12 J. J. Pignatello, E. Oliveros and A. MacKay, Advanced Oxidation Processes for Organic Contaminant Destruction Based on the Fenton Reaction and Related Chemistry, *Critical Reviews in Environmental Science and Technology*, 2006, **36**, 1-84.
- 13 W. W. Cleland, Dithiothreitol, a New Protective Reagent for SH Groups, *Biochemistry*, 1964, **3**, 480-482.
- 14 A. Giuffrè and J. B. Vicente, Hydrogen Sulfide Biochemistry and Interplay with Other Gaseous Mediators in Mammalian Physiology, *Oxid. Med. Cell. Longevity*, 2018, **2018**, 6290931.
- 15 S. Vasdev and V. Gill, Antioxidants in the Treatment of Hypertension, *Int J Angiol*, 2005, **14**, 60-73.
- 16 J. Rost and S. Rapoport, Reduction-potential of Glutathione, *Nature*, 1964, **201**, 185-185.